Biochimica et Biophysica Acta 932 (1988) 52–70
Elsevier

BBA 42665

Unidirectionality of charge separation in reaction centers of photosynthetic bacteria

M.E. Michel-Beyerle [a], M. Plato [b], J. Deisenhofer [c], H. Michel [c], M. Bixon [d] and J. Jortner [d]

[a] *Institut für Physikalische und Theoretische Chemie, Technische Universität München, Garching (F.R.G.),* [b] *Institut für Molekülphysik, Freie Universität Berlin, Berlin (Germany),* [c] *Max-Planck-Institut für Biochemie, Martinsried (F.R.G.) and* [d] *Sackler Faculty of Exact Sciences, School of Chemistry, Tel-Aviv University, Tel-Aviv (Israel)*

(Received 31 March 1987)
(Revised manuscript received 17 August 1987)

Key words: Electronic superexchange coupling; Reaction center; Charge separation; Electron transfer unidirectionality; Frank–Condon factor

Time-resolved spectroscopy in conjunction with X-ray structural data for reaction centers of *Rhodopseudomonas viridis* and *Rhodobacter sphaeroides* reveal a branching ratio $a > 5$ for the primary electron-transfer rates, favouring one of the two, almost symmetrical pigment/protein branches, L and M. In this paper we explore the origins of this unidirectionality of electron transfer between the excited singlet state of the bacteriochlorophyll dimer ($^1P^*$) and the bacteriopheophytin (H) along the L protein subunit. Nonadiabatic electron-transfer theory is applied to analyze the asymmetry of the electron-transfer rates, k_L and k_M across the L and M branches. The asymmetry originates from the cumulative contributions of the nuclear Franck–Condon factor and the electronic coupling, both of which enhance the electron transfer rate across the L branch. The nuclear Franck–Condon factors are modified by the energy difference ΔE_{LM} between the states $P^+H_L^-$ and $P^+H_M^-$, which is induced by the electrostatic interactions of these ion-pair states with the protein polar groups, as well as by asymmetric Coulomb and medium polarization interactions. The computation results in $\Delta E_{LM} = -(0.09 \pm 0.04)$ eV, which yields a nuclear enhancement contribution at 300 K of 1.5 (+0.8, −0.3) to k_L/k_M and therefore is insufficient to explain alone the observed asymmetry in reaction centers of *Rps. viridis*. Another contribution to the unidirectionality originates from electronic superexchange coupling for $^1P^*$-B-H via the virtual states of the accessory bacteriochlorophyll (B). The ratio of the intermolecular $^1P^*$-B_L and $^1P^*$-B_M electronic interaction terms was evaluated utilizing the tight-binding approximation with SCF-MO wavefunctions, together with the structural data for the prosthetic groups and for the polar amino acid side chains of the protein in reaction centers of *Rps. viridis*. The contribution to the enhancement of k_L/k_M by the electronic superexchange is approx. 8 ± 4. This asymmetry was traced to the combination of an excess negative charge density on the M-dimer component P_M, together with structural asymmetry, which enhances the P_M-B_L electronic overlap. Consequently, the $^1P^*$-B_L-H_L superexchange is favoured over the $^1P^*$-B_M-H_M interaction. The combined effects of asymmetric nuclear Franck–Condon factors and electronic couplings yield a branching ratio of the electron-transfer rates along the two pigment branches in reaction centers of *Rps. viridis* of an approx. 12 (−7, +15). This is sufficiently large to explain the experimentally observed unidirectionality.

Abbreviations: RC, reaction center; P, bacteriochlorophyll dimer consisting of two components: P_L and P_M (L for light weight, M for medium weight protein subunits); B, accessory bacteriochlorophyll; H, bacteriopheophytin; D, electron donor; A, electron acceptor; AAR, amino acid residue; SCF-MO, self-consistent-field-molecular-orbital.

Correspondence: M.E. Michel-Beyerle, Institut für Physikalische und Theoretische Chemie, Technische Universität München, Lichtenbergstrasse 4, 8046 Garching, F.R.G.

005-2728/88/$03.50 © 1988 Elsevier Science Publishers B.V. (Biomedical Division)

Introduction

The crystallographic data for the reaction center (RC) of the photosynthetic bacterium *Rhodopseudomonas viridis* [1] resulted in extensive information concerning the spatial arrangement of the prosthetic groups involved in the primary charge separation events. These prosthetic groups include four bacteriochlorophyll-*b* (B), two bacteriopheophytin-*b* (H) and two quinone molecules which are located in the two protein subunits, M (medium weight) and L (light weight), forming the M and L branches of the RC. The two branches exhibit an approx. 2-fold rotation symmetry (Fig. 1). Two B molecules very close to the rotation axis exhibit a short interplanar distance of approx. 0.3 nm, thus forming a dimer P (the 'special pair' [2,3]). Next to each of the dimer components P_L and P_M are the accessory monomers B_L and B_M followed in each branch by an H molecule. The sequence of prosthetic groups in the two branches is terminated by quinones, one of which being lost during the crystallization of the RC. Thus, the structure of the RC of *Rps. viridis* reveals that the spatial and orientational ordering of the pigments are almost identical in the two branches. One outstanding problem is the unidirectionality of the electron-transfer process along the L branch of the RC. The experimental evidence for the gross unidirectional charge separation in the RC rests on the following experimental observations.

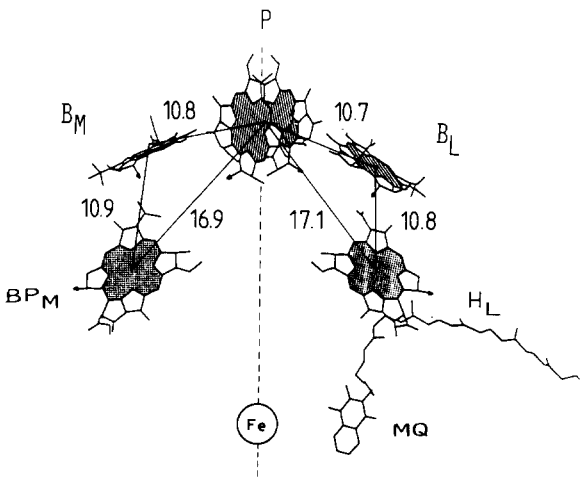

Fig. 1. An overview of the structure of the prosthetic groups in the RC of *Rps. viridis* [1]. The centre-to-centre distances are given in 10^{-1} nm with an accuracy of ± 0.02 nm.

Specific reduction of the bacteriopheophytin at the L branch

Recent femtosecond time-resolved studies of the RCs of *Rhodobacter sphaeroides* [5,6] and *Rps. viridis* [7] which were excited to the singlet state of the dimer, $^1P^*$, revealed that the photooxidation of P and the reduction of H occur simultaneously with a half lifetime of 2.8 ± 0.2 ps and no evidence exists for the kinetic involvement of the accessory B as an electron acceptor in these RCs [5–7], as already suggested by picosecond time-resolved data [8]. Only one H molecule is reduced in the primary electron-transfer process as already shown in previous picosecond time-resolved absorption measurements [9,10]. The Q_x electronic excitations of H_L and of H_M are different, being located at 543 nm and at 530 nm, respectively. Electron transfer from $^1P^*$ results in the bleaching of the 543 nm band of H_L, while the 530 nm band of H_M is immune to bleaching, providing evidence for the selective formation of H_L^-. Taking into account the strong overlap of the Q_x transitions of H_L and H_M at room temperature and the sensitivity of picosecond absorption experiments, a lower limit for the branching ratio of the primary electron-transfer rates, k_L and k_M from $^1P^*$ to H_L and to H_M, respectively, exceeds $k_L/k_M > 5$ for RCs of *Rps. viridis* and *Rb. sphaeroides*.

Chemical evidence

In RCs of *Rb. sphaeroides*, R-26, specific chemical reduction of the accessory bacteriochlorophyll [11] at the M branch * does not modify the rate for the primary electron transfer [12] from $^1P^*$ to H_L, providing further evidence for the dominance of this route of charge separation.

Delayed fluorescence from $^1P^*$

The time-resolved, low yield multiexponential fluorescence from RCs of *Rps. viridis* [13,14] and

* Recent resonance Raman studies on RCs of *Rb. sphaeroides*, R-26, identified the reduced bacteriochlorophyll monomer with the one at the M branch (Beese, D., Steiner, R., Scheer, H., Robert, B. and Lutz, M., Photochem. Photobiol., in press).

Rb. sphaeroides [15] can be explained in terms of parallel electron transfer along the L and M branches with a branching ratio for the primary electron-transfer rates being $k_L/k_M \simeq 6$ for *Rps. viridis,* so that the dominating route of charge separation would occur across the L branch.

The unidirectionality of the primary charge separation across the L branch is surprising in view of the nearly symmetric configuration of the prosthetic groups in the two branches, which are characterized by an (approximate) overall C_2 symmetry. A scrutiny of the detailed spatial and orientational arrangement of the pigments ('structural engineering') and of the environmental effects of the protein medium is required to elucidate the causes for the unidirectionality of the electron transfer process. The characterization and specification of the structural and environmental effects require information on the spatial ordering of the prosthetic groups, which is similar in *Rps. viridis* [1] and in *Rb. sphaeroides* [16] as well as information on the distribution of the protein residues in the RC which is currently available for *Rps. viridis* [17,18]. In what follows we shall invoke the basic assumption that the RCs of different purple bacteria have essentially similar structures. The paradigmatic structure is that of the RC of *Rps. viridis.*

In this paper we explore the unidirectionality of electron transfer in the RC assessing both the implications of 'structural engineering' of the prosthetic groups and the specific environmental effects exerted by the protein medium. On the basis of a recent analysis [19,20] we assert that dynamic protein medium effects on electron transfer, which originate from vibrational excitation and relaxation of the medium parallel to the electron-transfer process, are of minor importance for the primary reaction in the RC. This state of affairs prevails when the medium induced vibrational excitation and relaxation processes are fast on the time scale of the microscopic electron-transfer processes from the relevant vibronic levels [19,20]. Under these circumstances the electron transfer dynamics can be described in terms of conventional nonadiabatic theory [21–23].

We shall now proceed to address some of the possible sources of asymmetry in the dynamics of primary charge separation in the RC.

(1) The most natural cause of asymmetry is the difference in the energies of reaction along the two branches. Such differences result from shifts in the energies of the ion-pair P^+H^-, which are induced by specific interactions with the protein polar groups as well as from asymmetric Coulomb and medium polarization interactions. Changes in the reaction energies influence the reaction rates through the modification of activation energies. It will be shown in the Section Asymmetric electrostatic stabilization of ion-pair states that this cause of asymmetry is not sufficient to explain the observed unidirectionality.

(2) A second, and less obvious source of asymmetry could be traced to the electronic coupling elements. Due to the almost exact C_2 symmetry of the prosthetic groups no asymmetry is expected in the direct coupling between $^1P^*$ and P^+H^-. The asymmetry arises in the superexchange mechanism [24–36] which is much more sensitive to small structural and environmental differences.

Electron-transfer dynamics

In order to establish the origin of the asymmetry in the electron-transfer rate constant for the primary charge separation between the L and M branches in the RC we shall start from the basic equations and check the possible contributions of different parameters. The general formal expression for the nonadiabatic electron-transfer rate constant is given [23,27] as

$$k = \frac{2\pi}{\hbar}|V|^2 F \tag{1}$$

V is the electronic interaction term and F is the thermally averaged Franck–Condon nuclear overlap factor.

Nuclear Franck–Condon factors

First, we consider the nuclear overlap. Provided that the frequencies of the nuclear modes, $\hbar\omega$, are sufficiently low relative to the thermal energy $k_B T$, where k_B is the Boltzmann factor, the classical high-temperature limit of F is applicable, being given by the Marcus relation [37]:

$$F = (4\pi\lambda k_B T)^{-1/2} \, e^{-E_a/k_B T} \tag{2}$$

where the activation energy E_a is given by

$$E_a = \frac{(\Delta E - \lambda)^2}{4\lambda} \tag{3}$$

λ is the medium reorganization energy and ΔE is the (free) energy gap between the initial and final states in their equilibrium geometries *. For the primary electron-transfer process involving P and other prosthetic groups which contain porphyrin groups, the distortions of the nuclear configurations, which accompany electron transfer originate mainly from the protein modes [38]. For these nuclear protein modes in the RC it was estimated [38] that $\hbar\omega \approx 100\ cm^{-1}$ so that Eqn. 2 holds at room temperature.

The electron-transfer rate is then given by

$$k = \frac{2\pi V^2}{\hbar}(4\pi\lambda k_B T)^{-1/2}\, e^{-E_a/k_B T} \tag{4}$$

Electronic coupling

We shall now focus on the primary electron-transfer process between $^1P^*$ and H, which may proceed via alternative mechanisms, for example:

(i) sequential electron transfer $^1P^*BH \rightarrow P^+B^-H \rightarrow P^+BH^-$, with the participation of B^- as a kinetic intermediate [39]; and

(ii) single-step electron transfer $^1P^*BH \rightarrow P^+BH^-$, which is mediated by superexchange interactions (Refs. 24, 40, 64 and 65; see also Bixon, M., Michel-Beyerle, M.E., Ogrodnik, A. and Jortner, J., unpublished data). A recent study [41] favoured the two-step sequential mechanism (i), assuming that the electronic superexchange interaction is too low to account for the primary electron-transfer rate. However, once the dependence of the electronic matrix element on the nuclear configuration is incorporated [4] the superexchange electronic interaction is sufficiently large to make mechanism (ii) plausible. Furthermore, the analysis of the temperature-independent exchange integral [4] for the P^+H^- radical pair, as inferred from magnetic-field dependent recombination dynamics in RCs of *Rb. sphaeroides* provides strong evidence against the sequential mechanism (i). We conclude that the primary electron-transfer process involves single-step electron transfer, with the electronic interaction term, V, being dominated by superexchange via a 'virtual' P^+B^- ion-pair state. Therefore, the analysis of this paper will be based on the superexchange mechanism.

The superexchange interaction $^1P^*$-B-H is described by the mixing of the mediating (singlet) ion pair state $|P^+B^-\rangle$ into the singlet excitation $|^1P^*B\rangle$ [40,42]. The mixed excited state is

$$|*\rangle = \alpha|^1P^*B\rangle + \beta|P^+B^-\rangle \tag{5}$$

where α and β are the mixing coefficients, which can be obtained from the secular equation

$$[E(^1P^*B) - E(*)]\alpha + V_{DS}\beta = 0$$

$$V_{DS}\alpha + [E(P^+B^-) - E(*)]\beta = 0 \tag{6}$$

where $E(^1P^*B)$, $E(P^+B^-)$ and $E(*)$ are the energies of the states $|^1P^*B\rangle$, $|P^+B^-\rangle$ and $|*\rangle$, respectively, while V_{DS} is the electronic coupling between the donor state and the mediating state

$$V_{DS} = \langle ^1P^*B|\mathscr{H}|P^+B^-\rangle \tag{7}$$

with $\mathscr{H}$ being the electronic Hamiltonian of the system. When the energy gap $\delta E_{DS} = E(P^+B^-) - E(^1P^*B)$ exceeds V_{DS}, the first-order perturbative expression for β applies, with

$$\beta = \frac{V_{DS}}{\delta E_{DS}} \quad \text{for } \alpha \approx 1 \tag{8}$$

It is important to emphasize that δE_{DS} is the energy gap at the nuclear configuration of the intersection between the final and the initial nuclear potential surfaces. The electronic interaction, which appears in Eqn. 1 is

$$V = \langle *|\mathscr{H}|P^+H^-\rangle \tag{9}$$

Making use of Eqns. 5 and 9 one gets

$$V = \alpha V_{DA} = \beta V_{SA} \tag{10}$$

where

$$V_{DA} = \langle ^1P^*B|\mathscr{H}|P^+H^-\rangle \tag{11}$$

* As shown in the footnote on p. 58 the energy change ΔE equals the free-energy change ΔG for reaction centers of *Rb. sphaeroides*.

$$V_{SA} = \langle P^+ B^- H | \mathscr{H} | P^+ BH^- \rangle \quad (12)$$

Eqns. 8 and 10 yield the perturbative result

$$V \approx V_{DA} + \frac{V_{DS} V_{SA}}{\delta E_{DS}} \quad (13)$$

which corresponds to a sum of direct donor/acceptor interaction and of indirect coupling via the mediating B state. The P-B and B-H distances are considerably shorter than the P-H distance (Fig. 1). In view of the exponential dependence of V_{DS}, V_{SA} and V_{DA} on the distance between the relevant prosthetic groups one expects that for a sufficiently small energy gap the second term in Eqn. 13 dominates, resulting in

$$V = \frac{V_{DS} V_{Sa}}{\delta E_{DS}} \quad (14)$$

Eqn. 14 corresponds to the superexchange-induced electronic interaction.

Ratio of electron-transfer rate constants along the L and M branches

As we are interested in the asymmetry between the L and M branches at ambient temperatures let us investigate the expression for the ratio of the two electron-transfer rate constants k_L and k_M according to

$$\frac{k_L}{k_M} = \left| \frac{V_L}{V_M} \right|^2 \left(\frac{\lambda_M}{\lambda_L} \right)^{1/2} e^{-(E_{aL} - E_{aM})/k_B T} \quad (15)$$

Evidently each branch L (or M) is characterized by three parameters V_L (or V_M), λ_L (or λ_M) and E_{aL} (or E_{aM}). The activation energy, in turn, is expressed in terms of the energy of reaction ΔE_L (or ΔE_M) and the reorganization energy λ_L (or λ_M) according to Eqn. 3.

Eqn. 15 provides a general expression for the ratio of the rates k_L/k_M in the nonadiabatic high-temperature case. In view of the similarity of the protein structure we shall assert that $\lambda_M \approx \lambda_L$ and explore the consequences of asymmetry in the energetics and electronic coupling of the electron-transfer process on the ratio k_L/k_M. The asymmetry in the activation energies E_{aL} and E_{aM} is determined by the differences in the energies of reactions ΔE_L and ΔE_M, which originate from specific interactions of $P^+ H_L^-$ and $P^+ H_M^-$ with the protein medium. The specification and characterization of these environmental effects requires detailed structural information on the distribution of the polar protein residues in the RC, which will be summarized in the next Section and is utilized in the section thereafter to estimate the energetics of the charge-transfer states across the L and M branches and their contributions to k_L/k_M. The second ingredient which may contribute to the modification of k_L/k_M, Eqn. 15, is an asymmetry in the electronic coupling terms V_L and V_M. In the Section Electronic coupling we shall explore both geometric and environmental effects on the electronic coupling term.

The specific protein environment of the prosthetic groups

The RC complex of *Rps. viridis* consists of three distinguishable regions: the central part (core) containing prosthetic groups associated with the L and M protein subunits, a globular cytochrome and a globular H subunit. The L and M proteins in the core constitute a mostly nonpolar environment, being essentially devoid of charges and polar groups, with several notable exceptions, which pertain to the specific environment of several prosthetic groups. The following structural information [17,18] regarding the specific environmental features of the pigments is relevant for the elucidation of the electrostatic control mechanism:

The dimer environment

The dimer is surrounded by several polar amino acid residues (Fig. 2). The P_L component of P has a histidine group (L 173) bound to Mg^{2+}, another histidine group (L 168) hydrogen bound to the acetyl group and a threonine (L 248) bound to the carbonyl group of ring V. The P_M component of P has a histidine group (M 200) bound to Mg^{2+}, and a tyrosine group (M 195) which is hydrogen bound to the acetyl. There is asymmetry in the distribution of the protein polar groups with respect to the P_L and P_M components of the dimer.

The environment of the accessory bacteriochlorophylls

The Mg atoms of both B's are liganded to

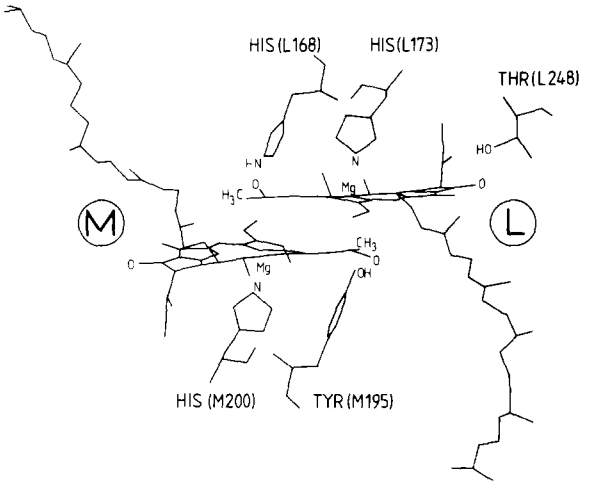

Fig. 2. Polar amino acid residues around the dimer in RCs of *Rps. viridis*. [18].

histidine residues (B_L to L 153 and B_M to M 180). There is a considerable number of Van der Waals interactions, but in contrast to the dimer and the bacteriopheophytins hydrogen bonds between the B's and the surrounding amino acid residues are not formed. In RCs of the carotinoidless mutant of *Rb. sphaeroides* a clear qualitative difference exists between B_L and B_M. The M branch B_M is preferentially reduced by sodium borohydride, whereas B_L remains essentially intact. X-ray crystallography on RCs of *Rps. viridis* shows an elongated feature in contact with the B_M molecule which may be the carotenoid.

The environment of the bacteriopheophytins

For the H_L and the H_M prosthetic groups a striking environmental asymmetry is exhibited with regard to the distribution of both nonpolar and polar amino acid residues (Figs. 3 and 4). Concerning aromatic residues, the H_L is surrounded by three phenylalanine groups (L 97, L 121 and L 241), while H_M has a single phenylalanine (M 148) in its immediate vicinity. Pointing away into the direction of the dimer we find a tyrosine (M 208) and a phenylalanine (L 181) close to H_L and H_M, respectively. Regarding polar residues, both H_L and H_M have a single tryptophane group (L 100 and M 127) in their vicinity, which in both cases is hydrogen bonded to the ester groups of ring V. Most important, the

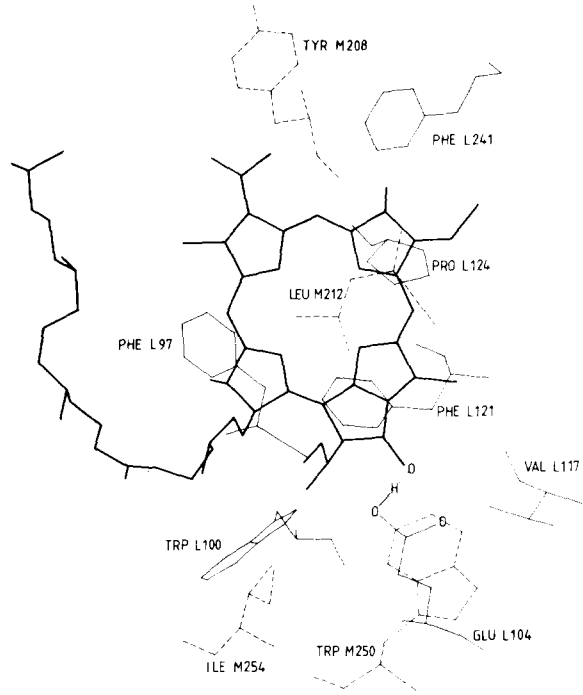

Fig. 3. The protein environment of H_L in RCs of *Rps. viridis* [18].

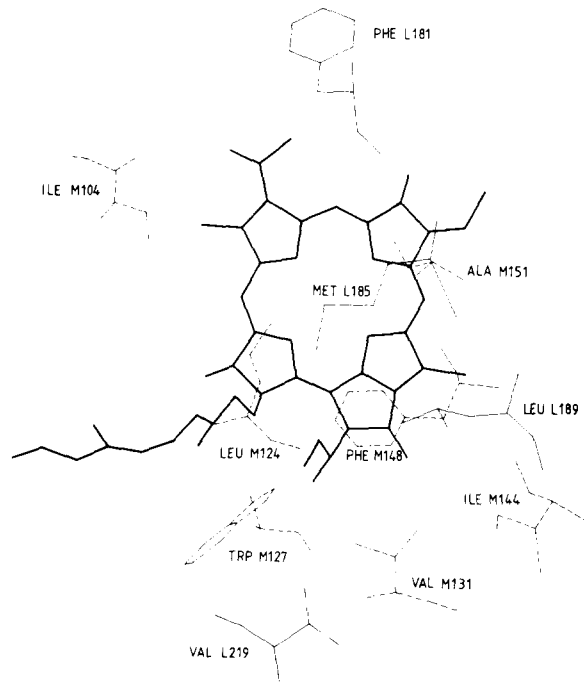

Fig. 4. The protein environment of H_M in RCs of *Rps. viridis* [18].

H_L has a polar glutamate side chain (L 104) in its vicinity, which is replaced in the M branch by a nonpolar valine (M 131). There exists considerable sequence homology [43] of the L and M subunits of RCs of *Rps. viridis, Rb. sphaeroides* and *Rb. capsulata,* having in common a glutamate side chain next to H_L. This glutamate is protonated, as evident from two pieces of spectroscopic data. Firstly, vibrational spectroscopic data for RCs of *Rb. sphaeroides* [44] show a redshifted keto-carbonyl frequency of H_L indicating intermolecular hydrogen bonding while H_M is free of hydrogen bonding to its keto-carbonyl. Accordingly, the glutamate side chain which is selectively bound to H_L is protonated (distance between the keto-oxygen at ring V of H and the protonated carboxyl-oxygen at the glutamate is approx. 0.29 nm). Secondly, new ENDOR data on H^- [45] in RCs of *Rb. sphaeroides* show that hydrogen/deuterium exchange occurs for weakly coupled protons on nearby amino acid residues. A preliminary analysis indicates that a probable candidate for the exchangeable proton is the hydrogen bond proton between the glutamic amino acid residue and the carbonyl oxygen on ring V of H_L.

Asymmetric electrostatic stabilization of ion-pair states

We shall now proceed to examine the energetics of the primary electron-transfer process from $^1P^*$ to H, considering its contribution to the ratio of the nuclear Franck–Condon factors in Eqn. 15.

Estimate of the energetic parameters required for $k_L/k_M > 5$

The available information regarding the numerical values of the energetic parameters is rather scarce. There is a wide scattering of experimental data for the energy of reaction on the L branch, ΔE_L. For *Rb. sphaeroides* ΔE_L = 1200–2200 cm^{-1} *, while for *Rps. viridis* $\Delta E_L \approx$ 2000 cm^{-1} [15]. We shall take 1200 $cm^{-1} \leq \Delta E_L \leq$ 2000 cm^{-1}.

An estimate for the reorganization energy λ_L can be inferred from the value of ΔE_L combined with the experimental observation that the electron-transfer rate is almost temperature independent down to cryogenic temperatures. This activationless behaviour limits the values of λ_L to the range 500 $cm^{-1} \leq \lambda_L \leq$ 1800 cm^{-1} in case ΔE_L = 1000 cm^{-1} and 1200 $cm^{-1} \leq \lambda_L \leq$ 3500 cm^{-1} in case ΔE_L = 2000 cm^{-1}. From the analysis of electron-transfer reactions in the RC [38], other than $^1P^*H \rightarrow P^+H^-$, we do not expect $\lambda <$ 1500 cm^{-1}. Therefore, we shall take λ_L to be in the range 1500 $cm^{-1} \leq \lambda_L \leq$ 3000 cm^{-1}.

We begin with the rate-enhancement factor that involves the ratio of the activation terms in Eqn. 15 $r = \exp\{-(E_{aL} - E_{aM})/k_BT\}$. We calculated the difference of the values of the heat of reactions in the L and M branches, $\Delta E_{LM} = \Delta E_L - \Delta E_M$, which are required to obtain numerical factors of 2, 4 and 6 for k_L/k_M within a range of experimental values for ΔE_L and λ_L. We have assumed that the reorganization energy has the same value for the two branches ($\lambda_L = \lambda_M = \lambda$). Fig. 5 represents the results of such calculations, each curve gives the dependence of ΔE_{LM} on ΔE_L for given values of λ and the rate enhancement factor r. Fig. 5 presents only those parts of the curves that are consistent with the activationless property of the electron-transfer reaction. One immediate result that can be inferred from Fig. 5, is that in order to obtain a factor of 5 for k_L/k_M the change in reaction energy, ΔE_{LM}, must exceed 1000 cm^{-1} for ΔE_L = 1500 cm^{-1} and ΔE_{LM} must exceed 1500 cm^{-1} for ΔE_L = 2000 cm^{-1}.

It is possible to obtain alternative estimates for ΔE_{LM} by using the recent experimental measure-

* Experimental estimates for ΔG_L in RCs *Rb. sphaeroides,* were reported as 1600 cm^{-1} [46] and 1850 cm^{-1} [14] at room temperature. (In addition, Ref. 46 gives a value $\Delta G^* \approx$ 1200 cm^{-1} for an initial, unrelaxed charge separated state P^+H^-.) Taking the energy difference between the singlet ($^1P^*$) and the triplet ($^3P^*$) excitations of the dimer as approx. 3200 cm^{-1} [47,48] together with its temperature independence [48] and the value $\Delta G \approx$ 1300 cm^{-1} for the free-energy gap between P^+H^- and $^3P^*$, one obtains $\Delta G_L \approx$ 1850 cm^{-1} in good consistency with the above data from time-resolved fluorescence measurements. $\Delta G(P^+H^-\text{-}^3P^*)$ has been derived from magnetic-field and temperature-dependent recombination data and triplet lifetimes [49] in the theoretical framework of spin dynamics (Ogrodnik, A., Remy-Richter, N. and Michel-Beyerle, M.E., unpublished results). Since $\Delta G(P^+H^-\text{-}^3P^*)$ has been shown to be almost temperature independent in the range 230–295 K, ΔG and ΔE are assumed to be about equal at room temperature.

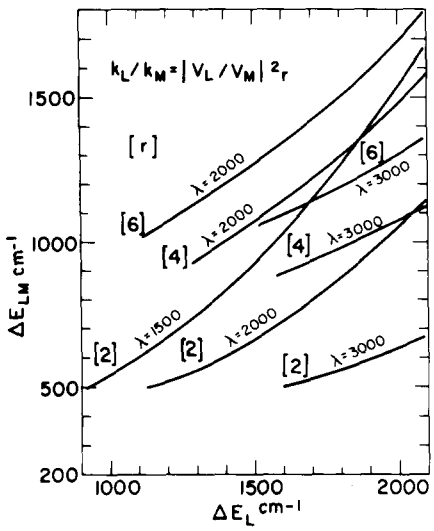

Fig. 5. The dependence of the nuclear enhancement factor, r, of the electron-transfer rate along the L branch at 300 K on the energy of reaction ΔE_L for the L branch, on the difference between the energies of reaction ΔE_{LM} for the L and M branches and on the reorganization energy λ in cm^{-1}. These data correspond to (nearly) activationless electron transfer.

ments of the rate constants of the first charge-separation steps in intact and reduced RCs in *Rps. viridis*. The only difference between the two systems is the negative charge on the quinone in the reduced state. The electrostatic interaction of this extra charge with the radical pair $P^+H_L^-$ changes its energy and diminishes the electron-transfer rate. The observed electron-transfer times are 2.8 ± 0.2 ps for the intact and 6.0 ± 0.9 ps for the reduced state [6,50,51]. The ratio of the rate constants is $k_{intact}/k_{red} = 2.1 \pm 0.4$. Contributions to this ratio may originate from protein-conformational changes induced by the presence of Q^- and from electrostatic interactions. We shall show that the latter contribution results in energetic parameters, which are consistent with those emerging from the previous analysis of Fig. 5. To calculate the electrostatic interaction energy $\Delta(\Delta E)$ between Q^- and P^+H^- we use the crystallographic results which give the value 1.4 nm for the center-to-center distance between the quinone and H_L and 2.8 nm for the distance between the quinone and the dimer. We obtain $\Delta(\Delta E) = \varepsilon^{-1}\ 4.1 \cdot 10^3$ cm^{-1} = ε^{-1} 0.51 eV, where ε is the effective dielectric constant, which is taken in the range $3 \leq \varepsilon \leq 4$ [52]. This limits the change, $\Delta(\Delta E)$, in reaction energy for electron transfer in the untreated RC and in the quinone-reduced RC to the range 1000 cm$^{-1} < \Delta(\Delta E) \leq 1400$ cm^{-1}. The ratio $k_{intact}/k_{red} \approx 2.1$ together with this range for $\Delta(\Delta E)$ limits us according to Fig. 5 to the range of parameters 1400 cm$^{-1} \leq \Delta E_L \leq 2100$ cm^{-1} and 1500 cm$^{-1} \leq \lambda \leq 2100$ cm^{-1}. In this range of parameters an asymmetry factor $r \approx 5$ would require a change in reaction energies of $\Delta E_{LM} \approx 1600$ cm^{-1} = 0.2 eV.

Energy difference between $P^+H_L^-$ and $P^+H_M^-$ ion-pair states

We shall now proceed to evaluate the difference between the energies of the ion-pair states produced in the primary charge separation process

$$\Delta E_{LM} = E(P^+H_L^-) - E(P^+H_M^-) \tag{16}$$

by analyzing all possible contributions. The final result for ΔE_{LM} will have to be compared with the required value of 0.2 eV as estimated. Estimate of the energetic parameters required for $k_L/k_M > 5$, earlier in this Section.

We are interested in the energy $E(D^+A^-)$ of an ion-pair state D^+A^-, where D and A refer to the electron donor and electron acceptor, respectively. The calculation of the energies of the ion-pair states in the RC will be based on the conceptual frame-work developed for the energies of analogous ion-pair states in molecular crystals [53,54]. Invoking the well-known relationship [53,54] for $E(D^+A^-)$

$$E(D^+A^-) = I - EA + p + C + \delta\varepsilon(D^+) - \delta\varepsilon(D) + \delta\varepsilon(A^-) - \delta\varepsilon(A) \tag{17}$$

where I is the ionization potential of the donor P, EA is the electron affinity of the acceptor H, p is the polarization energy of the nonpolar protein medium by D^+ and A^-. $\delta\varepsilon(D^+)$ and $\delta\varepsilon(A^-)$ are the electrostatic stabilization energies of D^+ and A^-, respectively, which originate from the interaction of charges on the prosthetic groups with polar protein residues. Finally, $\delta\varepsilon(D)$ and $\delta\varepsilon(A)$ are the electrostatic stabilization energies of D and A, respectively, which originate from the interaction of the polar neutral prosthetic groups with the polar protein residues.

Only partial information exists regarding the

numerical values of the energetic parameters I, EA and p, which is summarized in Appendix A. The uncertainties in these energetic values exceed the expected energy difference ΔE_{LM}. Accordingly, the calculation of the absolute energies of the ion-pair states will not provide us with helpful information. A better strategy is to evaluate directly the energy differences between the ion-pair states, Eqn. 16. Taking the energy differences according to Eqn. 17 it is apparent that the contribution of the terms I, EA and $\delta\varepsilon(P^+) - \delta\varepsilon(P)$ to ΔE_{LM} cancels out because they are identical for both ion-pair states $P^+H_L^-$ and $P^+H_M^-$. The resulting energy difference is

$$\Delta E_{LM} = C(P^+H_L^-) - C(P^+H_M^-) + p(P^+H_L^-) - p(P^+H_M^-) + \{\delta\varepsilon(H_L^-) - \delta\varepsilon(H_L)\} - \{\delta\varepsilon(H_M^-) - \delta\varepsilon(H_M)\} \quad (18)$$

Consequently, the energetic contributions to ΔE_{LM} originate from:

(a) the difference between the electrostatic stabilization energies of H_L^- and H_M^- by the polar residues in the vicinity of each negatively charged group;

(b) the difference between the Coulomb energies for the states $P^+H_L^-$ and $P^+H_M^-$;

(c) the difference in protein polarization around H_L^- and H_M^-.

Difference in electrostatic stabilization energies. The electrostatic stabilization energies were calculated using an atomic charge model for the ions of the prosthetic groups and for the amino acid polar residues. This requires the net atomic charges and the atomic coordinates. Atomic charge densities of P, P^+, H and H^- were calculated by the well-known semi-empirical 'INDO' SCF-MO method by Pople and Beveridge [57] which includes all valence electrons. A spin-restricted version of this method, known as 'half-electron (HE)' method [58] was used for the charged radical species. The summation of the electron populations over occupied molecular orbitals on a given atom j gives the gross electron population P_{jj} on this atom. The net atomic charge q_j is obtained by subtracting P_{jj} from the core charge z_j. The entire molecular structures of the prosthetic groups were taken except for truncation of the phytyl chain on ring IV. This chain does not participate in the π-system and will not undergo any significant changes in its charge distribution. Fig. 6 shows the difference of the net atomic charge distributions of H and H^- revealing significant accumulation of negative charge at the keto-group of ring V.

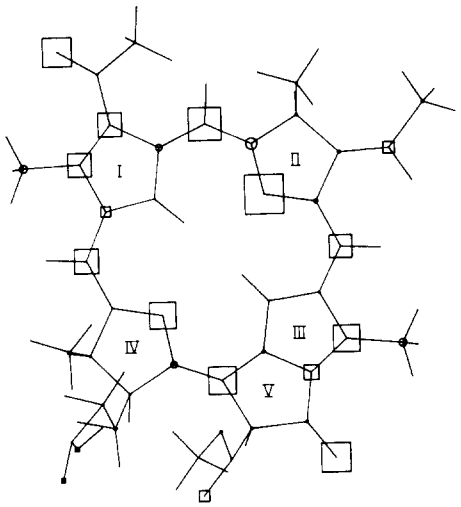

Fig. 6. Difference in charge densities on the 'bare' H^- and H calculated in the geometry given by the X-ray structure of RCs of *Rps. viridis* [18]. ○, +0.50; □, −0.50; △, charge density.

The coordinates of the atoms of the prosthetic groups and the protein polar residues (the previous Section) were obtained from the crystallographic data [18]. The uncertainty of the experimental data for the atomic coordinates is ±20 pm, so that the uncertainty in the interatomic distances is $\Delta R = 40$ pm. The coordinates of the protons on the polar amino acid residues, e.g., the glutamate in the vicinity of H_L, were calculated using the empirical geometric parameters of Scheraga and coworkers [59]. The carboxyl group of protonated glutamate near the H_L was taken to lie on a straight line between the carbonyloxygen on ring V of H_L and the carboxyloxygen of glutamate next to it. For the O–H distance in the glutamate carboxy group we adopted the value of 0.1 nm which is typical for a hydrogen bond with a heavy atom distance of 0.29 nm [18].

The electrostatic stabilization energies $\delta\varepsilon(Y)$ were obtained from the simple relation

$$\delta\varepsilon(Y) = e^2 \sum_i \sum_k \frac{q_i^Y q_k^{AAR}}{R_{ik}} \qquad (19)$$

$Y = P, P^+, H_{L(M)}, H^-_{L(M)}$

which accounts for the unscreened electrostatic interaction between each amino acid residue (AAR) and the charged and uncharged prosthetic groups. As we shall consider only electrostatic interactions between a P^+ or H^- group and nearest-neighbour polar residues no dielectric screening of these interactions is necessary. Stated in alternative terms the effective local dielectric constant for these short distances is close to unity. Therefore, we obtain upper limits for the stabilization energies. In Eqn. 19 q_i^Y are the net atomic charges on Y, q_k^{AAR} are the atomic charges on the particular AAR, while R_{ik} are distances between atom i on Y and atom k on the AAR. We note in passing that these electrostatic interactions (Eqn. 19) assume the asymptotic form of charge-dipole interactions falling off at large distances as R_i^{-3}. Furthermore, at larger separation dielectric screening by the static dielectric constant of the protein, $2 < \varepsilon < 4$ [52], reduces this electrostatic interaction. Consequently, $\delta\varepsilon(Y)$ were dominated by interaction with the nearest polar AARs adjacent to Y.

The electrostatic stabilization of the dimer (Appendix B) does not contribute to the asymmetry of the energetics of charge separation. The electrostatic stabilization of H_L^- and of H_M^- is of considerable interest. The contributions to $\delta\varepsilon(H_L^-)$ arise from the GLU (L 104) and from TRP (L 100). Table I summarizes the electrostatic interaction energies of H_L^- and of H_L with GLU (L 104). For the deprotonated GLU these interactions are repulsive resulting in significant destabilization of H_L^-. On the basis of experimental vibrational [44] and ENDOR [45] spectroscopic data on RCs of *Rb. sphaeroides* the glutamate is protonated and its interaction (Table I) stabilizes the H_L^- state. The contributions to $\delta\varepsilon(H_M^-)$ originate from TRP (M 127) and from the polar OH group of the TYR (M 208), which points away from H_M and its energetic contribution is small ($|\delta\varepsilon| \leq 0.01$ eV).

TABLE I

ELECTROSTATIC INTERACTION ENERGIES OF GLU (L 104) WITH H_L^- AND H_L

System	$\delta\varepsilon$ (eV)
H_L/Glu (deprotonated)	$+0.113 \pm 0.02$
H_L^-/Glu (deprotonated)	$+0.535 \pm 0.04$
H_L/Glu (protonated)	-0.074 ± 0.02
H_L^-/Glu (protonated)	-0.123 ± 0.02
Electrostatic stabilization energy of H_L^- by Glu (protonated)	-0.05 ± 0.02

These calculations reveal that (1) the electrostatic stabilization of H_M^- is $(\delta\varepsilon(H_M^-) - \delta\varepsilon(H_M)) < 0.01$ eV, being negligible; (2) electrostatic stabilization is exhibited for H_L^- originating from its interaction with the protonated glutamate and (3) the total stabilization energy of H_L^- is

$$\delta\varepsilon(H_L^-) - \delta\varepsilon(H_L) \approx -(0.05 \pm 0.02)\ \text{eV} \qquad (20)$$

The electrostatic calculations are based on the configurational information derived from the crystallography of the RC in its equilibrium ground state. The protein relaxes in response to changes in the charge distribution on the prosthetic groups. In principle, the calculation of the electrostatic stabilization of P^+H^- should be based on the relaxed protein geometry around it, but such configurational information is not available. As long as changes in the hydrogen bond distance of the protonated glutamate to the keto-group of ring V of H do not exceed 10–20 pm, the energy of the hydrogen bond does not change by more than 30%, which is comparable to the uncertainty in our results (Table I). In this case the contribution of extra stabilization caused by relaxation would not affect our conclusions.

Difference in the Coulomb energies. We turn now to the evaluation of the Coulomb energy C between the charged prosthetic groups. According to our MO-calculations the P^+ dimer is characterized by an asymmetric charge distribution with $Q_L = +0.56\ e$ on P_L and $Q_M = +0.44\ e$ on P_M. Consequently, the Coulomb stabilization energies of the $P^+H_L^-$ and $P^+H_M^-$ will be different with a preferable stabilization of the former state. As the Coulomb energy involves long-range interactions between two molecular ions whose centers are separated by approx. 1.7 nm, dielectric screening by the static protein dielectric constant ε has to be incorporated. The Coulomb energy is ex-

pressed in terms of atom–atom interactions

$$C = e^2\varepsilon^{-1}\sum_i\sum_j \frac{q_i q_j}{R_{ij}} \tag{21}$$

where q_i and q_j are the net atomic charges on atom i of P^+ and atom j on H^- (in units of e), respectively, while R_{ij} is the distance between atoms i and j. The Coulomb energies C_L and C_M for the ion-pair states $P^+H_L^-$ and $P^+H_M^-$, respectively, were calculated to be

$$C_L = -\frac{0.80\pm0.03}{\varepsilon}\text{ eV and } C_m = -\frac{0.73\pm0.03}{\varepsilon}\text{ eV}$$

with the uncertainty originating again from the experimental inaccuracy in the atomic coordinates. Using $\varepsilon = 3$ [52] we estimate

$$C_L = -(0.27\pm0.01)\text{ eV and } C_M = -(0.24\pm0.01)\text{ eV}$$

Thus, there is a small asymmetric contribution of the Coulomb energy,

$$\Delta C = C_L - C_M = -(0.022\pm0.01)\text{ eV} \tag{22}$$

Difference in medium polarization energies. Another contribution to the environmental stabilization of H_L^- relative to H_M^- may result from polarization energies. The available structural data show clearly that on the L branch there is a larger density of aromatic amino acids. Two extra phenylalanins are closer to H_L relative to H_M. The aromatic groups have larger polarizabilities and therefore we may expect higher polarization energy for H_L^-. It is impossible to calculate the difference in polarization energies but we can attempt rough estimates. As estimated in Appendix A the polarization energy due to one H^- is about 1 eV. A rough geometrical estimation shows that two phenyl groups occupy less than 8% of the available space around H. Their polarizability (due to higher atomic density) is about 30% higher than that of aliphatic chains, so we have an overall correction of less than 2.4% out of 1 eV so that

$$\Delta p \approx -(0.02\pm0.02)\text{ eV} \tag{23}$$

Energetic contribution to asymmetry of Franck–Condon factors

The total asymmetric electrostatic energy ΔE_{LM}, Eqn. 18, can now be evaluated in the form

$$\Delta E_{LM} = \delta\varepsilon(H_L^-) - \delta\varepsilon(H_L) + \Delta C + \Delta p \tag{24}$$

Using the numerical estimates of the energetic contributions as given in Eqns. 20, 22 and 23 we obtain

$$\Delta E_{LM} = -(0.09\pm0.03)\text{ eV}$$

This value of ΔE_{LM} together with $\Delta E_L = \lambda = 1600\text{ cm}^{-1}$ indicates (Fig. 5) that the contribution of the asymmetry in the energetics of the ion-pair states $P^+H_L^-$ and $P^+H_M^-$ to the ratio k_L/k_M results in an enhancement factor $r \approx 1.5(+0.8, -0.3)$ at 300 K. Obviously, the enhancement factor of the nuclear contribution increases at low temperatures assuming the value of $r \approx 2.7(+5.4, -1.3)$ at 100 K. However, the asymmetry in the energetics of the ion pair cannot account for the unidirectionality of the charge separation at room temperature. This nuclear contribution to the ratio k_L/k_M is in the right direction, but it is too small in its absolute value to account for the experimental asymmetry. We have to explore other contributions to the ratio k_L/k_M, which will be undertaken in the next section.

Electronic coupling

From the analysis of the preceding sections we infer that the selective electrostatic stabilization of the ion-pair state $P^+H_L^-$, although not negligible, cannot account quantitatively for the observed large asymmetry of the electron-transfer rates, k_L and k_M. Thus, the modification of the nuclear Franck–Condon factors is not sufficient to account for the unidirectionality of the charge separation. According to Eqn. 15 the remaining source of asymmetry in the charge separation across the L branch is a difference between the electronic coupling terms V_L and V_M. A grossly simplified description of the electronic coupling term involves the exponential distance dependence [22,23]

$$V = A\,e^{-\alpha R} \tag{25}$$

where R is the center-to-center donor-acceptor separation. Orientational effects can be included by taking V to be proportional to the overlap integral S_{ij} of p_z orbitals for π-systems, i.e.,

$$V \propto \cos\theta \tag{26}$$

Eqn. 25 seems to be applicable both to direct exchange [22,23] and to superexchange [28], with the exponent α being lower in the latter case, with a value of $\alpha \approx 7$ nm^{-1}. The structural data [18] show that the center-to-center distances ($R = 1.7 \pm 0.01$ nm) as well as the angles ($\theta = 100 \pm 1°$) between the normals to the planes of rings I of the dimer are equal for $P_L - H_L$ and $P_M - H_M$ within the errors of the atomic coordinates (± 20 pm). The corresponding uncertainty for $|V_L/V_M|^2$ following from Eqns. 25 and 26 ranges from 0.6 to 1.5 which is inadequate to account for the observed asymmetry.

From this simple analysis we infer that the heuristic expressions Eqns. 25 and 26, although useful as guidelines, are inadequate to probe fine details of the intermolecular electronic coupling. In particular, the present case, with superexchange electronic coupling dominating (see Section Electron-transfer dynamics), requires a more elaborate treatment of the electronic coupling.

The superexchange coupling of $^1P^*$ with H_L and of $^1P^*$ with H_M involves the accessory bacteriochlorophylls, B_L and B_M, which form bridging elements on both the L and the M branches, as discussed in the section Electron-transfer dynamics. The electronic superexchange coupling may be different across the L and M branches due to the following effects:

(A) Electronic asmmetry. Asymmetry of the charge distribution of $^1P^*$ originating from both the structure of the 'bare' dimer and from the interaction of the highly polar dimer with the polar amino acid residues.

(B) Geometrical asymmetry. Geometrical effects of the spacing and orientation of the $^1P^*$ donor relative to the mediating accessory bacteriochlorophylls. In view of the spatial proximity of P and B and of B and H, the electronic coupling terms, which determine the superexchange interaction, Eqn. 14, are very sensitive to small local geometrical differences.

(C) Energetic asymmetry. The superexchange interaction, Eqn. 14 is inversely proportional to the energy gap $\delta\varepsilon_{DS}$. The energy gaps are expected to be asymmetric due to the environmental differences of B_L and B_M (subsection The environment of the accessory bacteriochlorophylls (pages 56 and 57)).

The superexchange interaction, Eqn. 14, depends on the $^1P^*$-B electronic coupling V_{DS}, on the B-H electronic coupling V_{SA} and on the energy gap $\delta\varepsilon_{DS}$. We assume that the V_{SA} interactions are practically identical for the L and M branches, since the shortest heavy-atom distances r_{SA} are equal on both branches within 10 pm when restricting the comparison to π-centers and methyl carbons. The asymmetry in the superexchange interactions can therefore be expressed as

$$\left|\frac{V_L}{V_M}\right|^2 = \left|\frac{V_{DS}(L)}{V_{DS}(M)}\right|^2 \left|\frac{\delta\varepsilon_{DS}(M)}{\delta\varepsilon_{DS}(L)}\right|^2 \tag{27}$$

The first term $\psi = |V_{DS}(L)/V_{DS}(M)|^2$ gives the contribution of the electronic coupling between the $^1P^*$ donor and the mediating states $P^+P_L^-$ and $P^+B_M^-$, and is sensitive to the electronic and geometrical asymmetry on the L and M branches. The second term $\chi = |\delta\varepsilon_{DS}(M)/\delta\varepsilon_{DS}(L)|^2$ expresses the contribution of the energetic asymmetry.

Origin of electronic asymmetry

Strong indication for the asymmetry of the charge distribution on $^1P^*$ is obtained from SCF-MO-INDO calculations of the type RHF-INDO/SP [57,60]. We have performed spin-density and charge-density calculations on P^+ and $^1P^*$ using the X-ray structural data of *Rps. viridis*. The perturbing electrostatic effect of surrounding polar amino acid residues on the MO's of the dimer has been accounted for by including Coulomb interaction terms of the form $\Sigma q_j/r_{ij}$ in the Fock matrix, where q_j is the net atomic charge on any amino acid atom j and r_{ij} is the distance from atom i on the dimer and atom j. The values of q_j were taken from Scheraga's CNDO results [59] on the isolated amino acid residues.

These SCF-MO calculations predict a significant asymmetry of spin-density on the monomeric halves P_L and P_M (ratio 1.7 : 1) of the dimer cation P^+. This asymmetry is also revealed by the experimental spin density distribution determined from isotropic hyperfine couplings by ENDOR in solution techniques [61]. A reversal of this asymmetry is predicted for the radical P^- anion. Accordingly,

the lowest excited singlet state $^1P^*$, which is characterized by two electrons residing in approximately the same orbitals as the unpaired electrons of the two ion radicals P^+ and P^-, is expected to have considerably more negative charge on P_M than on P_L. In Table II we present a sample of the atomic charge densities obtained from SCF-MO calculations on the two combined components, P_L and P_M of the 'bare' dimer and of the $^1P^*$ dimer interacting with the polar amino acid residues. An overview of the dimer charge distribution is provided in Fig. 8. These results demonstrate two effects. Firstly, there is a surplus negative charge density on P_M relative to P_L. Secondly, the negative charge density on P_M is enhanced by the electrostatic interaction with the polar amino acid residues. To provide a quantitative measure of the electronic asymmetry we have calculated the total charges

$$Q_L^* = \sum_{i \in P_L} Q_i \text{ and } Q_M^* = \sum_{j \in P_M} Q_j$$

on the P_L and P_M components of $^1P^*$, resulting in $Q_L^* = +0.36$ and $Q_M^* = -0.36$ for the 'bare' dimer (lacking C_2-symmetry), while $Q_L^* = +0.54$ and $Q_M^* = -0.54$ for the dimer interacting with the polar groups (all values given in units of $|e|$). Accordingly, the electronic charge asymmetry is enhanced by approx. 50% due to the interactions with the polar protein medium. This enhancement

TABLE II

SOME ATOMIC CHARGE DENSITIES ON $^1P^*$

The notation of atoms is according to Fig. 7.

Atom	Bare		With polar residues	
	L branch	M branch	L branch	M branch
Mg	0.462	0.467	0.490	0.504
C_{11}	0.151	0.102	0.162	0.089
C_1	0.004	−0.031	0.016	−0.038
C_{2a}	0.300	0.292	0.303	0.296
O_6	−0.339	−0.357	−0.355	−0.377
C_{9a}	0.029	0.012	0.039	0.004
C_9	0.309	0.301	0.315	0.300
O_1	−0.334	−0.358	−0.349	−0.361
N_{II}	−0.233	−0.289	−0.237	−0.280
N_{IV}	−0.226	−0.262	−0.222	−0.270
O_4	−0.345	−0.361	−0.344	−0.360

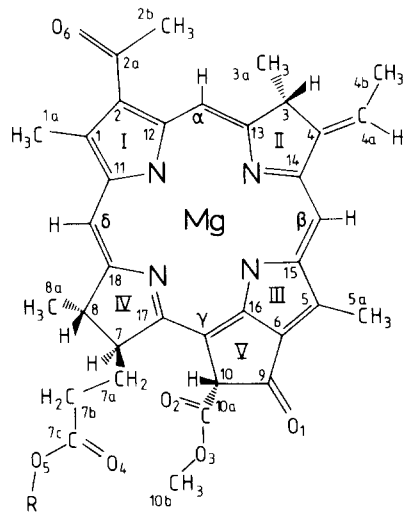

Fig. 7. Molecular structure and labelling of atoms of bacteriochlorophyll-*b*.

is not only due to the presence of the asymmetrically placed amino acid residue, THR L 248, but to the combined action of all surrounding polar groups.

Origin of structural asymmetry

Inspection of the available X-ray data for the relative atom–atom distances of the dimer at the two accessory bacteriochlorophylls reveals rather surprisingly that B_L is closer to P_M than to P_L. This is evident from the nearest heavy-atom distances between P and the accessory Bs (Table III). It should be noted that the distance of 0.345 nm given for the pair P_L-B_L involves an atom (O_4) on the dimer which is 5 bonds away from the π-system, whereas all the other distances refer to atoms

TABLE III

NEAREST HEAVY ATOM DISTANCES BETWEEN THE DIMER AND THE ACCESSORY BACTERIOCHLOROPHYLLS, EXCLUDING THE PHYTYL CHAIN

The notation of atoms is as in Fig. 7.

Prosthetic groups	Atoms	Distance (nm)
P_L-B_L	O_4-C_{4b}	0.345
P_L-B_M	O_6-C_{5a}	0.375
P_M-B_L	C_{2b}-C_{5a}	0.326
P_M-B_M	C_9-C_{4b}	0.340

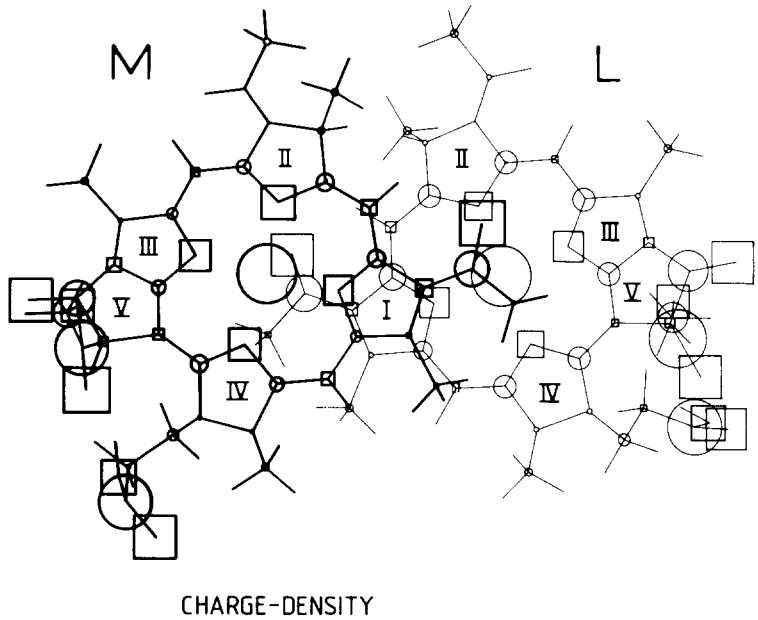

Fig. 8. Charge density on the excited singlet state of the bacteriochlorophyll-*b* dimer $^1P^*$ calculated in the geometry given by the X-ray structure of *Rps. viridis* [18] including interaction with the polar amino acid residues. ○, +0.300; □, −0.300.

belonging to the π-system or at most one bond away (methyl carbons). The structural asymmetry seems to favour the $^1P^*$-B_L over the $^1P^*$-B_M electronic coupling due to closer proximity of the P_M component of $^1P^*$ with B_L. If hydrogen atoms are added to methyl carbons, assuming tetrahedral structure and $r_{CH} = 0.109$ nm, the closest atom-to-atom distances reduce to approx. 0.19 and 0.24 nm for P_M-B_L and P_M-B_M, respectively.

Origin of energetic asymmetry

The energy gaps $\delta\varepsilon_{DS}$ may be different due to significant differences in the environments of B_L and B_M (subsection The environment of the accessory bacteriochlorophylls, pages 56 and 57). In principle, the energy difference may be estimated along the lines of the Section Asymmetric electrostatic stabilization of ion-pair states. However, the existing incomplete structural information precludes such calculations. At present we can only assert that this effect may contribute to the asymmetry of the superexchange interaction. As is discussed in a forthcoming paper (Bixon, M., Michel-Beyerle, M.E., Ogrodnik, A. and Jortner, J., unpublished results), $\delta\varepsilon_{DS}$ is estimated to be of the order of a few hundred cm^{-1}. Then small absolute energy differences would result in large effects. For the time being we shall assume, in the absence of any experimental evidence, that $\chi = 1$. This potential contribution may either increase or decrease the asymmetry of the superexchange interaction.

Calculations of the electronic coupling

From the combination of the electronic asymmetry which enhances excess negative charge density on P_M, together with the structural asymmetry which enhances the P_M-B_L electronic overlap we can assert that $^1P^*$-B_L-H_L superexchange interaction is favoured over the $^1P^*$-B_M-H_M interaction. Both the electronic asymmetry and the structural asymmetry contribute to the relative increase of the superexchange interaction along the L branch, which, surprisingly enough, is caused by the enhancement of the P_M^*-B_L coupling.

We shall now proceed to provide numerical estimates for the electronic coupling terms $V_{DS}(L)$ and $V_{DS}(M)$ terms. The starting point for the electron transfer process can be (approximately) described as

$$(H_M)(B_M)(P_L^{\delta+} P_M^{\delta-})^*(B_L)(H_L)$$

with $\delta = 0.54$, where the individual species are ordered according to their spatial proximity. The electronic coupling integral V_{DS} can be numerically calculated by using the tight-binding approximation with SCF-MO wavefunctions, which are represented by a linear combination of atomic orbitals [62,63]. This procedure gives [63]

$$V_{DS} = \sum_i \sum_j C_i^D C_j^S H_{ij}^{DS} \tag{28}$$

where C_i^D and C_j^S are the coefficients of the highest occupied MO's on the atoms i of $^1P^*$ and j of B^-, and H_{ij}^{DS} are the electronic matrix elements of the intermolecular Coulomb interaction between $^1P^*$ and B involving the atomic orbitals i and j. The values of the MO coefficients C_i^D and C_j^S were taken from the SCF-MO INDO calculations [60] using the X-ray structure data of *Rps. viridis*. These calculations include 1-s orbitals of hydrogen atoms which were attached to the heavy atom skeleton by standard rules [57]. The matrix elements H_{ij}^{DS} were taken to be proportional to the intermolecular overlap integrals S_{ij} of the atomic orbitals i and j, in analogy to the parametrization of non-diagonal matrix elements (resonance integrals) in the conventional INDO procedure [57]

$$H_{ij}^{DS} = KS_{ij} \tag{29}$$

where K is a numerical constant. This approach should give roughly the distance and orientation dependence of H_{ij}.

The V_{DS} integral, Eqn. 27 is thus approximated by

$$V_{DS} \approx K \sum_i \sum_j C_i^D C_j^S S_{ij} \tag{30}$$

We have evaluated the intermolecular atomic overlap integrals S_{ij} in Eqn. 30 using Slater orbitals with a single orbital exponent. This is certainly a poor description for the absolute values of these integrals, which are determined by the tails of the wavefunctions. These long-range tails are underestimated using a single Slater orbital [63]. However, this approximation is reasonable for the description of relative values of the V_{DS} terms *. We have used this procedure to evaluate the ratio

$$\frac{V_{DS}(L)}{V_{DS}(M)} = \frac{\sum_{i \in {}^1P^*} \sum_{j \in B_L^-} C_i^D C_j^S S_{ij}}{\sum_{i \in {}^1P^*} \sum_{j \in B_M^-} C_i^D C_j^S S_{ij}} \tag{31}$$

with i and j referring again to the HOMOs of $^1P^*$ and H_L^- or of H_M^-. Convergence of $V_{DS}(L)$ and $V_{DS}(M)$ within a few percent was achieved by including all pairs of atomic orbitals i and j with a separation $r_{ij} < 0.5$ nm, the number of the terms in Eqn. 30 being about 10^3. These numrical calculations resulted in

$$\psi = \left| \frac{V_{DS}(L)}{V_{DS}(M)} \right|^2 = 8 \pm 4 \tag{32}$$

which provides a semiquantitative estimate for the total asymmetry of the electronic coupling. The uncertainty of $\pm 50\%$ originates from the inaccuracy of ≈ 0.02 nm of the atomic coordinates used in this work (medium refinement). It is interesting at this stage to decompose the total electronic coupling terms into their individual contributions from the two components of the dimer

$$V_{DS}(L) = V(P_L - B_L) + V(P_M - B_L) \tag{33}$$

$$V_{DS}(M) = V(P_L - B_M) + V(P_M - B_M) \tag{34}$$

where $V(P_I - B_J)$ with $I = L, M$ and $J = L, M$ is the electronic coupling between the Ith component of the B dimer with the Jth of the accessory B. In Table IV we present the relative magnitudes of the individual contributions to Eqns. 32–34 which indicate that the dominant contribution to $V_{DS(L)}$ originates from $V(P_M - B_L)$, while about equal contributions to $V_{DS(M)}$ come from $V(P_M - B_M)$ and from $V(P_L - B_M)$.

* Calculation are in progress to determine better values for the ratio of the $V_{DS}(L)$ and $V_{DS}(M)$ couplings using SCF LCAO molecular wavefunctions with the atomic orbital being represented by accurate SCF multiple-zeta 2p orbitals. This procedure is expected to account properly for the behaviour of the molecular wavefunctions at large distances relevant to the problem.

TABLE IV

CONTRIBUTIONS (IN ARBITRARY UNITS) TO THE ELECTRONIC COUPLING INTEGRALS BETWEEN $^1P^*$ AND THE ACCESSORY BACTERIOCHLOROPHYLLS-*b*

Group of dimer	Prosthetic group	Contribution to V_{DS} (arbitrary units)
P_M	B_L	−1.00
P_L	B_L	−0.12
P_L	B_M	+0.23
P_M	B_M	+0.17

Conclusions

From our analysis we assert that the unidirectionality of the charge separation across the L branch of the RC in *Rps. viridis* originates from the combination of the structural engineering and specific environmental effects which enhance k_L relative to k_M. Each of these nonadiabatic electron-transfer rates corresponds to a product of an electronic superexchange term and a nuclear overall Franck–Condon factor, both of which are enhanced across the L branch in the following manner:

Contribution to nuclear Franck–Condon factors

The energetic contribution to the Franck–Condon factor results in a rate enhancement factor, $r = 1.5$ $(+0.8, -0.3)$ at room temperature.

Contributions to the electronic coupling

(1) Structural asymmetry originating from the relatively small differences in the spatial arrangement of the components of P relative to H_L and H_M.
(2) Electronic asymmetry due to the asymmetry of the charge distribution of the 'bare' $^1P^*$, which originates from the dimer structure.
(3) Enhancement of electronic asymmetry due to the interaction of $^1P^*$ with the polar protein residues.

The contribution of both structural (1) and electronic asymmetry (2 and 3) effects to the rate enhancement is $\psi = 8 \pm 4$. The total enhancement of the unidirectionality of the electron transfer across the L branch is $a = k_L/k_M = \psi r \chi$. In our analysis we were unable to estimate the contribution of the energy gap asymmetry to the electronic coupling. Setting $\chi = 1$ yields $k_L/k_M = 12$ $(-7, +15)$ at room temperature.

From the experimental point of view it may be possible to distinguish between the asymmetries of the electronic coupling and the nuclear Franck–Condon factor on the basis of their temperature dependence. The contribution of the asymmetry of the electronic coupling is temperature independent, provided that the effects of the local protein structure on the electronic asymmetry are not affected by temperature changes. On the other hand, the contribution to the asymmetry of the nuclear Franck–Condon factor is expected to exhibit a marked temperature dependence, being enhanced at lower temperatures. However, regarding the large value of k_L/k_M at room temperature very accurate experimental data will be required to distinguish between these two contributions.

With respect to general methodology it should be noted that our estimates of the distinct contributions ψ and r rest on the experimental information for the ordering of the prosthetic groups and for the distribution of the polar protein residues in RCs of *Rps. viridis*. The recent data [16] on the structure of RCs of *Rb. sphaeroides* R-26, indicate that indeed the spatial ordering of the prosthetic groups may be universal in purple photosynthetic bacteria. However, some fine details of the spatial ordering of the pigments and of the distributions of the polar residues may quantitatively affect the three distinct contributions r, ψ and χ to the asymmetry of k_L/k_M of charge separation in RCs of different bacteria.

Appendix A. Energies of ion-pair states

We shall utilize Eqn. 17 to estimate the energy of the $P^+H_L^-$ state relative to the ground state PH_L. Some partial information of the energetic parameters I, EA and p in Eqn. 17 is currently available. Theoretical calculations of the ionization potential of bacteriochlorophyll *b* yield $I =$ 6.2 eV (Plato, M., unpublished results) in accord with the experimental values for I in the range 5.9–6.3 eV for various porphyrins [55]. I for the prophyrin dimer is yet unknown. The theoretical calculations of the electron affinities yield $EA =$

1.76 eV for B and $EA = 1.60$ eV for H (Plato, M., unpublished results).

The polarization energy p for a pair of large molecular ions in the nonpolar protein medium can be roughly estimated from the Born charging energy

$$p \simeq -\frac{e^2}{2R_1}\left(1-\frac{1}{\varepsilon_s}\right)-\frac{e^2}{2R_2}\left(1-\frac{1}{\varepsilon_s}\right) \qquad \text{(A-1)}$$

where R_1 and R_2 are the radii of the molecular ions. A more reliable estimate of p can be derived from experimental values [54] for ionization potentials and photoelectric thresholds in molecular crystals resulting in the p of approx. -2.4 to approx. -3.2 eV, while the most accurate value for crystalline anthracene seems to be approx. -2.75 eV [54]. This estimate is consistent with the measurements of the ionization potentials of porphyrins in the nonpolar isooctane solvent [56] which result in the medium polarization energy induced by a single ion $p_+ = -1.2$ eV, so that $p \simeq 2p_+ = -2.4$ eV. We conclude that p varies between approx. -2.4 and approx. -3.2 eV.

For the calculation of the energy of $P^+H_L^-$ we take: $I = 6.2$ eV and $EA = 1.6$ eV; both values with an uncertainty of 0.2 eV, $p = -2.8$ eV with an uncertainty of 0.4 eV, $C = -0.27$ eV from the subsection Difference in the Coulomb energies (page 61) with an uncertainty of 0.01 eV, $\delta\varepsilon(P^+) - \delta\varepsilon(P) = -0.03$ eV from Appendix B with an uncertainty of 0.01 eV and $\delta\varepsilon(H_L^-) - \delta\varepsilon(H_L) = -0.05$ eV from the subsection Difference in electrostatic stabilization energies (page 60) with an uncertainty of 0.02 eV. Eqn. 17 yields $E(P^+H_L^-) = (1.4 \pm 0.5)$ eV, where the conservative estimate of the uncertainty is taken as 50% of the sum of the uncertainties of all the individual energetic parameters. This energy is consistent with the experimental energy of $\simeq 1.1$ eV for $P^+H_L^-$ for RCs of *Rb. sphaeroides*. However, the large uncertainty in the estimates prevents the use of absolute energies of ion-pair states for estimates of nuclear Franck–Condon factors, which determine the *ET* rates.

Appendix B. Electrostatic stabilization of P^+

The evaluation of the electrostatic stabilization energy of the dimer cation $[\delta\varepsilon(P^+) - \delta\varepsilon(P)]$ was performed using Eqn. 19 together with the atomic charge densities and structural data mentioned in Sections The specific protein environment of the prosthetic groups and Asymmetric electrostatic stabilization of ion-pair states. The results for the electrostatic interactions of P^+ with the eight closest polar amino acid residues are present in Table V. These calculations show $\delta\varepsilon(P^+) = -(0.48 \pm 0.06)$ eV and $\delta\varepsilon(P) = -(0.45 \pm 0.06)$ eV. The uncertainties in energetics originate from the experimental uncertainties in the determination of the interatomic distances. Separating these energies into the individual interactions of the component P_L and P_M with the polar residues, i.e., $\delta\varepsilon(P) = \delta\varepsilon_L(P) + \delta\varepsilon_M(P)$ and $\delta\varepsilon(P^+) = \delta\varepsilon_L(P^+) + \delta\varepsilon_M(P^+)$, we get $\delta\varepsilon_L(P) = -0.23$ eV, $\delta\varepsilon_M(P) = -0.22$ eV, $\delta\varepsilon_L(P^+) = -0.22$ eV and $\delta\varepsilon_M(P^+) = -0.24$ eV. The stabilization energy of the dimer cation relative to the ground state P is thus extremely low,

$$\delta\varepsilon(P^+) - \delta\varepsilon(P) = -(0.03 \pm 0.01)\ \text{eV}$$

From these results we conclude that there is no asymmetry in the electrostatic stabilization of both P and P^+ and that there is a remarkable cancellation of the partial and total electrostatic stabilization energy of the dimer cation.

TABLE V

UNSCREENED ELECTROSTATIC INTERACTIONS OF P^+ AND OF P WITH POLAR RESIDUES (ENERGIES IN eV)

Residue	Interaction with P	Interaction with P^+
His L 173	−0.082	−0.097
His M 200	−0.111	−0.123
His L 168	−0.075	−0.038
Tyr M 195	−0.068	−0.074
Thr L 248	−0.071	−0.060
Tyr M 208	−0.013	−0.031
Val L 157	−0.006	−0.028
Ala M 278	−0.026	−0.025
Total energy	-0.450 ± 0.060	-0.477 ± 0.060

Acknowledgements

We are grateful to Dr. W. Lersch for conducting the first calculations on electrostatic sta-

bilization of ion-pair states in the reaction center and to Dr. E. Tränkle for many helpful discussions. We are indebted to Prof. S.F. Fischer who collaborated with us extensively on theoretical studies of the energetics and dynamics of the reaction center. We like to thank Professors K. Möbius, W. Lubitz and H. Scheer for prepublication information and for interesting discussions.

This research was supported by the Deutsche Forschungsgemeisnchaft (M.E. Michel-Beyerle within Sonderforschungsbereich 143 and M. Plato within Sonderforschungsbereich 337). J. Jortner would like to express his gratitude for the generous support by the Z. Weinberg Research Fund for Chemical Physics at Tel-Aviv University.

References

1 Deisenhofer, J., Epp, O., Miki, K., Huber, R. and Michel, H. (1984) J. Mol. Biol. 180, 385–398.
2 Norris, J.R., Uphaus, R.A., Crespi, H.L. and Katz, J.J. (1971) Proc. Natl. Acad. Sci. USA 68, 625–628.
3 Feher, G., Hoff, A.J., Isaacson, R.A. and Ackerson, L.C. (1975) Ann. NY Acad. Sci. 244, 239–259.
4 Bixon, M., Jortner, J., Michel-Beyerle, M.E., Ogrodnik, A. and Lersch, W. (1987) Chem. Phys. Lett. 140, 626–630.
5 Martin, J.-L., Breton, J., Hoff, A.J., Migus, A. and Antonetti, A. (1986) Proc. Natl. Acad. Sci. USA 83, 957–961.
6 Breton, J., Martin, J.-L., Petrich, J., Migus, A. and Antonetti, A. (1986) FEBS Lett. 209, 37–43.
7 Breton, J., Martin, J.-L., Migus, A., Antonetti, A. and Orszag, A. (1986) Proc. Natl. Acad. Sci. USA 83, 5121–5125.
8 Parson, W.W., Woodbury, N.W.T., Becker, M., Kirmaier, C. and Holten, D. (1985) in Antennas and Reaction Centers of Photosynthetic Bacteria (Michel-Beyerle, M.E., ed.), pp. 278–285, Spinger-Verlag, Berlin.
9 Rockley, M.G., Windsor, M.W., Cogdell, R.J. and Parson, W.W. (1975) Proc. Natl. Acad. Sci. USA 72, 2251–2255.
10 Kaufmann, K.J., Dutton, P.L., Natzel, T.L., Leigh, J.S. and Rentzepis, P.M. (1975) Science 188, 1301–1304.
11 Ditson, S.L., Davis, R.C. and Pearlstein, R. (1984) Biochim. Biophys. Acta 766, 623–629.
12 Maroti, P., Kirmaier, C., Wraight, C., Holten, D. and Pearlstein, R.M. (1985) Biochim. Biophys. Acta 810, 132–139.
13 Hörber, J.K.H., Göbel, W., Ogrodnik, A., Michel-Beyerle, M.E. and Knapp, F.W. (1985) in Antennas and Reaction Centers of Photosynthetic Bacteria (Michel-Beyerle, M.E., ed.), pp. 292–297, Springer-Verlag, Berlin
14 Hörber, J.K.H., Göbel, W., Ogrodnik, A., Michel-Beyerle, M.E. and Cogdell, R.J. (1986) FEBS Lett. 198, 268–272.
15 Hörber, J.K.H., Göbel, W., Ogrodnik, A., Michel-Beyerle, M.E. and Cogdell, R.J. (1986) FEBS Lett. 198, 273–278.
16 Allen, J.P., Feher, G., Yeates, T.O., Rees, D.C., Deisenhofer, J., Michel, H. and Huber, R. (1986) Proc. Natl. Acad. Sci. USA 83, 8589–8595.
Chang, C.H., Tiede, D., Tang, J., Smith, U., Norris, J. and Schiffer, M. (1986) FEBS Lett. 205, 82–86.
17 Deisenhofer, J., Epp, O., Miki, K., Huber, R. and Michel, H. (1985) Nature 318, 618–622.
18 Michel, H., Epp, O. and Deisenhofer, J. (1986) EMBO J. 5, 2445–2451.
19 Garg, A., Onuchic, J.N. and Ambegaokar, V. (1985) J. Chem. Phys. 83, 4491–4503.
20 Rips, I. and Jortner, J. (1987) J. Chem. Phys., in press
21 Levich, V.G. (1965) Adv. Electrochem. Eng. 4, 249–371.
22 Hopfield, J.J. (1974) Proc. Natl. Acad. Sci. USA 71, 3640–3644.
23 Jortner, J. (1980) J. Am. Chem. Soc. 102, 6676–6686.
24 Ogrodnik, A., Remy-Richter, N., Michel-Beyerle, M.E. and Feick, R. (1987) Chem. Phys. Lett. 135, 576–581.
25 McConnell, H.M. (1961) J. Chem. Phys. 35, 508–515.
26 Halpern, J. and Orgel, L.E. (1960) Disc. Farad. Soc. 29, 32–41.
27 Jortner, J. (1976) J. Chem. Phys. 64, 4860–4867.
28 Miller, J.R. (1985) in Antennas and Reaction Centers of Photosynthetic Bacteria (Michel-Beyerle, M.E., ed.), pp. 234–241, Springer-Verlag, Berlin.
29 Joran, A.D., Leland, B.A., Geller, G.G., Hopfield, J.J. and Dervan, P.B. (1984) J. Am. Chem. Soc. 106, 6090–6092.
30 Beratan, D.N. (1986) J. Am. Chem. Soc. 108, 4321–4326.
31 Heitele, H. and Michel-Beyerle, M.E. (1985) J. Am. Chem. Soc. 107, 8286–8287.
32 Heitele, H., Michel-Beyerle, M.E., Finckh, P. and Rettig, W. (1986) in Tunneling (Jortner, J. and Pullman, B., eds.), pp. 333–345, D. Reidel, Dordrecht.
33 Warman, J.M., De Haas, M.P., Paddon-Row, M.N., Cotsaris, E., Hush, N.S., Oevering, H. and Verhoeven, J.W. (1986) Nature 320, 615–616.
34 Larsson, S. and Volosov, A. (1986) J. Chem. Phys. 85, 2548–2553.
35 Closs, G.L., Calcaterra, L.T., Green, N.J., Penfield, K.W. and Miller, J.R. (1986) J. Phys. Chem. 90, 3673–3683.
36 Ohta, K., Closs, G.L., Morokuma, K. and Green, N.J. (1986) J. Am. Chem. Soc. 108, 1319–1320.
37 Marcus, R.A. (1956) J. Chem. Phys. 24, 966–978, 979–989.
38 Bixon, M. and Jortner, J. (1986) J. Phys. Chem. 90, 3795–3800.
39 Haberkorn, R., Michel-Beyerle, M.E. and Marcus, R.A. (1979) Proc. Natl. Acad. Sci. USA 70, 4185–4188.
40 Fischer, S.F., Nussbaum, I. and Scherer (1985) in Antennas and Reaction Centers of Photosynthetic Bacteria (Michel-Beyerle, M.E., eds.), pp. 278–285, Springer-Verlag, Berlin.
41 Marcus, R.A. (1987) Chem. Phys. Lett. 133, 471–477.
42 Jortner, J. and Bixon, M. (1986) Comments on Mol. Cell Biophysics 3, 387–406.
43 Michel, H., Weyer, K.A., Gruenberg, H., Dunger, I., Oesterhelt, D. and Lottspeich, F. (1986) EMBO J. 5, 1149–1158.
44 Lutz, M. and Robert, B. (1985) in Antennas and Reaction Centers of Photosynthetic Bacteria (Michel-Beyerle, M.E., ed.), pp. 138–145, Springer-Verlag, Berlin.

45 Feher, G., Isaacson, R.A., Okamura, M.Y. and Lubitz, W. (1987) Biophys. J. 51, 337a.
46 Woodbury, N.W.T. and Parson, W.W. (1984) Biochim. Biophys. Acta 767, 345–361.
47 Parson, W.W., Clayton, R.K. and Cogdell, R.J. (1975) Biochim. Biophys. Acta 387, 265–278.
48 Takiff, L. and Boxer, S.G. (1987) Photochem. Photobiol. 45, 61S.
49 Chidsey, C.E.D., Takiff, L., Goldstein, R.A. and Boxer, S.G. (1985) Proc. Natl. Acad. Sci. USA 82, 6850–6854.
50 Zinth, W., Nuss, M.C., Franz, M.A., Kaiser, W. and Michel, H. (1985) in Antennas and Reaction Centers of Photosynthetic Bacteria (Michel-Beyerle, M.E., ed.), pp. 286–291, Springer-Verlag, Berlin.
51 Wasielewski, M.R. and Tiede, D.M. (1986) FEBS Lett. 204, 368–371.
52 Warshel, A. and Russel, S.T. (1984) Q. Rev. Biophys. 17, 283–422.
53 Berry, R.S., Jortner, J., Mackie, J.S., Pysh, E.S. and Rice, S.A. (1965) J. Chem. 42, 1535–1540.
54 Pope, M. and Swenberg, C.E. (1982) Electronic Processes in Organic Crystals, p. 304, Clarendon Press, Oxford.
55 Dupuis, P.R., Roberge, R. and Sandorfy, C. (1980) Chem. Phys. Lett. 75, 434–437.
56 Nakoto, Y., Chogoda, T. and Tsubomura, H. (1976) Chem. Phys. Lett. 39, 358–360.
57 Pople, J.A. and Beveridge, D.L. (1970) Approximate Molecular Orbital Theory, McGraw-Hill, New York.
58 Dewar, M.J.S., Hashmall, J.A. and Venier, C.G. (1968) J. Am. Chem. Soc. 90, 1953–1963.
59 Nemethy, G., Pottle, M.S. and Scheraga, H.A. (1983) J. Phys. Chem. 83, 1883–1887.
60 Plato, M., Tränkle, E., Lubitz, W., Lendzian, F. and Möbius, K. (1986), Chem. Phys. 107, 185–196.
61 Lubitz, W., Lendzian, F., Plato, M., Tränkle, E. and Möbius, K. (1986) Proceedings of the College Ampère XXIII, Rome, 486–487.
62 Leblanc, O.H. (1960) J. Chem. Phys. 35, 1275–1280.
63 Katz, J.L., Rice, S.A., Choi, A.I. and Jortner, J. (1963) J. Chem. Phys. 39, 1683–1697.
64 Parson, W.W., Woodbury, N.W.T., Becker, M., Kirmaier, C. and Holten, D. (1985) in Antennas and Reaction Centers of Photosynthetic Bacteria (Michel-Beyerle, M.E., ed.), pp. 345–366, Springer-Verlag, Berlin.
65 Jortner, J. and Michel-Beyerle, M.E. (1985) in Antennas and Reaction Centers of Photosynthetic Bacteria (Michel-Beyerle, M.E., ed.), pp. 345–366, Springer-Verlag, Berlin.